Int J Adv Manuf Technol (2007) 32: 1211–1217
DOI 10.1007/s00170-006-0442-5

ORIGINAL ARTICLE

Du Zhiqiang · Zhou Zude · Ai Wu · Chen Youping

A linear drive system for the dynamic focus module of SLS machines

Received: 23 May 2005 / Accepted: 3 December 2005 / Published online: 21 March 2006

Abstract This paper presents a linear drive system that implements the high-accuracy reciprocating motion of the dynamic focus module in selective laser sintering (SLS) rapid prototyping manufacturing. The linear drive system consists of a moving-coil type PM linear DC motor (LDM), a DSP-based digital controller, a pulse-width modulated servo amplifier, and a linear optical encoder. The special configuration and dynamic model of the LDM are presented, the transfer function of the control system is derived, and a PID feedback controller including a low-pass filter with the derivative term and a model-based feedforward controller are designed. The present experiment proves that the tracking performance of the control system is satisfactory. The experimental results show that the linear drive system has fast dynamic response and acceptable tracking error in the driving dynamic focus module of SLS machines.

Keywords Linear drive system · Dynamic focus module · Position tracking control · Linear DC motor

1 Introduction

In selective laser sintering (SLS) rapid prototyping manufacturing, the desirable laser spot size should be uniform in the whole image field to achieve a high-quality prototyping profile. For the post-objective scanning system, when the ordinary objective lens is used to focus the laser beam, varying spot sizes can be found in a flat image field. In addition, there will be a different defocus error with a different scanning coordinate on the image field [1, 2]. To control the laser spot size and eliminate the defocus error, the dynamic focus module contains a lens cell (the dynamic expansion lens) that is adopted to adjust focusing rapidly, as shown in Fig. 1. It is a unique Z-axis scanning element that translates along its optical axis under the precise control of the linear translator in a three-axis laser galvanometric scanning system. Motion of the dynamic expansion lens varies the image range from the scan mirror and produces an exact focus at each coordinate of the flat field [3].

The conventional linear translator is a closed-loop servo motor with limited rotation. The coupling link transmission mechanism not only increases the complexity of the drive system, but it also introduces many nonlinear factors, such as friction, backlash, and elastic deformation, which cause difficulties in achieving high control accuracy. In order to achieve the desirable laser spot size more accurately and quickly, we experimented on using the moving-coil PM linear DC (LDM) motor instead of the rotary-to-linear conversion mechanism, since the motor possesses a good force–current linear relationship and low inertia, as well as fast dynamic response [4–6]. Moreover, the linear motion produced from a linear motor can eliminate the problems otherwise encountered in the conversion from rotary motion to linear motion, and can result in a more reliable and economical drive system [7, 8]. Although the rotary version is well reported [3], little information is documented concerning its linear equivalent.

The aim of this research is to develop a linear drive system for the dynamic focus module used in SLS rapid prototyping machines. This paper is organized as follows. Section 2 presents the configuration of the LDM and its dynamic model. Section 3 gives the control strategy for the linear drive system and the transfer function of the system. Section 4 describes the implementing method of the PID controller, including a low-pass filter with the derivative term and the feedforward controller. Section 5 illustrates the experimental results of position tracking control, while some conclusions are drawn in Section 6.

D. Zhiqiang (✉) · Z. Zude · A. Wu · C. Youping
Engineering Research Center of Numerical Control System,
School of Mechanical Science and Engineering,
Huazhong University of Science and Technology,
Wuhan, Hubei Province, 430074, People's Republic of China
e-mail: zqduhust@163.com

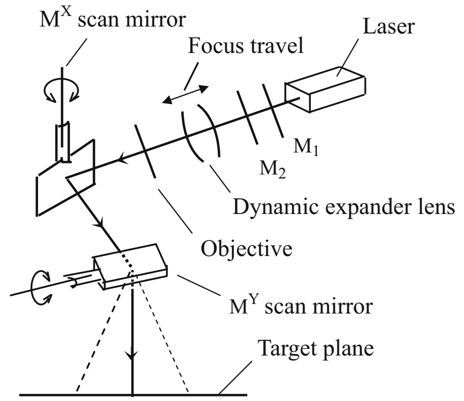

Fig. 1 A galvanometric scanning system

2 Actuator description

2.1 Construction and principle of operation

Figure 2 shows the cross-sectional view of the LDM. The moving coil mounted on the shaft is a tubular coil situated within a radially oriented magnetic field and balanced by the two opposing forces generated by the two springs along with the central axis. The magnetic field is produced by the two concentric ring permanent magnets embedded on the stator. The stator is used to complete the magnet circuit. The linear guide prevents the moving coil from rotating around on the central axis. The required controlled travel is limited in a ±5-mm displacement range.

The magnetic flux density in the gap acts on the moving coil current and generates thrust proportional to the moving coil current. The thrust, according to Fleming's rule, is in the direction of the stroke.

2.2 Dynamic model of the LDM

The dynamic behavior of the LDM can be expressed by the following equations. The equivalent circuit of the coil winding is shown in Fig. 3. The voltage equation can be presented as:

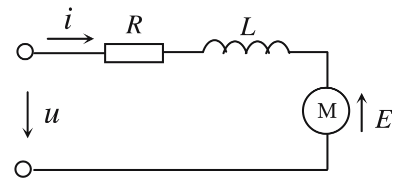

Fig. 3 Equivalent circuit for coil winding

$$u = iR + L\frac{di}{dt} + \frac{d\phi}{dx}\frac{dx}{dt} = iR + L\frac{di}{dt} + E \tag{1}$$

where u, i, R, L, ϕ, x, N, and E are the applied voltage, the electric current, the coil resistance, the coil inductance, the flux linkage in the coils, the coil displacement, the number of total turns, and the back-EMF, respectively. The back-EMF can be expressed as:

$$E = \frac{d\phi}{dx}\frac{dx}{dt} = k_b B_\delta l N \frac{dx}{dt} = k_E \frac{dx}{dt} \tag{2}$$

where B_δ and l are the magnetic flux density and the average length of each turn, respectively. k_b is the ratio between the permanent magnet length and the moving coil length. $\frac{dx}{dt}$ is the velocity of the moving coil and $k_E = k_b B_\delta l N$ is a back-EMF constant.

The electromagnetic force can be evaluated by calculating the rate of co-energy variation due to the coil displacement under constant current:

$$F_m = \frac{dw_m}{dx} = \frac{id\phi}{dx} = \frac{ik_b B_\delta l N dx}{dx} = k_b B_\delta l N i = k_m i \tag{3}$$

where F_m is the electromagnetic force and $k_m = k_b B_\delta l N$ is the thrust constant.

Since the driven load is the mass of the lens cell, the oscillatory dynamics of the LDM may be simplified as a system with a lumped mass, two springs, and two viscous

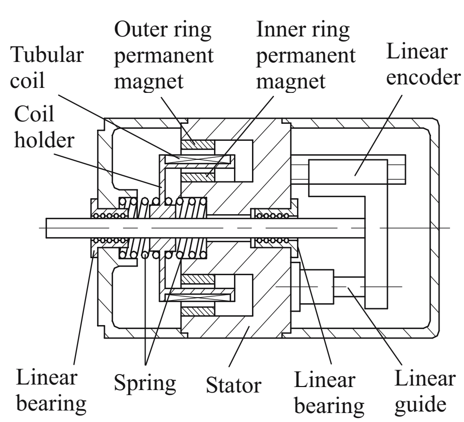

Fig. 2 Cross-sectional view of linear DC motor (LDM)

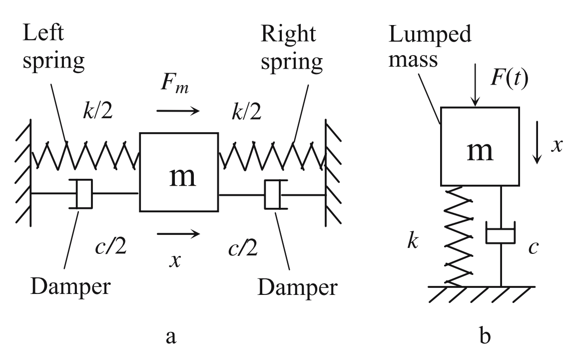

Fig. 4 a, b Lumped mass model of LDM. **a** Elementary model. **b** Equivalent model

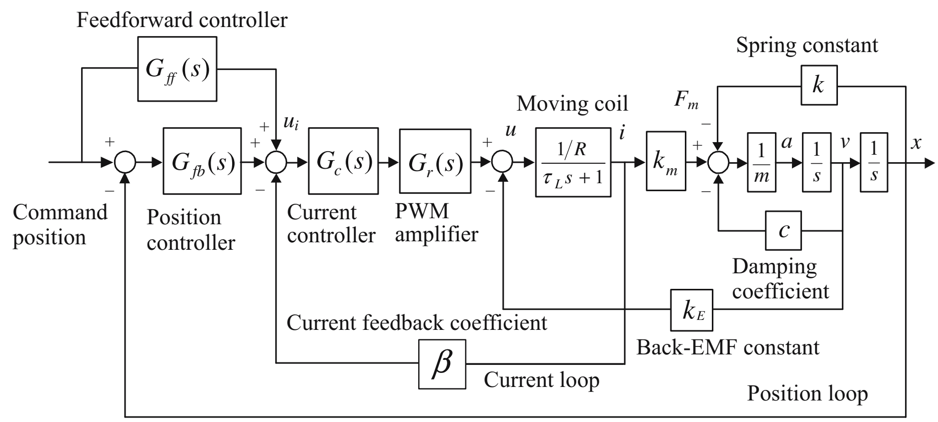

Fig. 5 Block diagram of the closed-loop control system

dampers, as shown in Fig. 4a. The equivalent model is shown in Fig. 4b. The motion equation of the mechanical system is:

$$m\frac{d^2x}{dt^2} + c\frac{dx}{dt} + kx = F_m \tag{4}$$

where m, c, and k are, respectively, the overall mass including the lens cell and the mover of the LDM, the viscous damping coefficient, and the complex spring constant.

3 Modeling of the linear drive system

Figure 5 shows the proposed control strategy for the linear drive system. It is a dual-loop cascade control structure with a position feedforward controller. The current loop intersects the back-EMF loop. In practice, since the electrical time constant of a drive is much smaller compared to the mechanical time constant of the LDM, and the rate of current variation is much faster compared with the rate of the back-EMF variation, the small electrical time constant and the back-EMF term in Eq. 1 can be ignored [9]. The transfer function of the current loop may be approximated as Eq. 5:

$$\frac{I(s)}{U_i(s)} \approx \frac{1}{\beta} = k_a \tag{5}$$

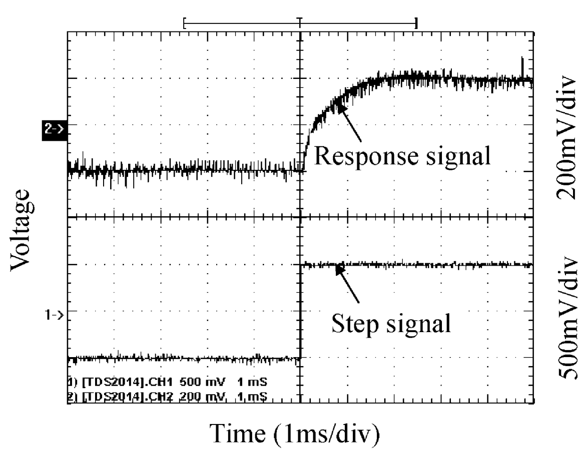

Fig. 6 Measured waveform of the current loop response

where β is the current feedback coefficient and k_a is the amplifier gain.

Equation 5 relates the amplifier input voltage to the current output of the coil winding. Figure 6 is the measured step response of the current loop. It can be seen that the electrical time constant is less than 1 ms. The scaling is 4 A/V in the response curve. Hence, the overall transfer function $G_P(s)$ between the amplifier input voltage $U_i(s)$ and the displacement $X(s)$ can be simplified as a second-order model as follows:

$$G_P(s) = \frac{X(s)}{U_i(s)} = \frac{k_a k_m}{ms^2 + cs + k} \tag{6}$$

Equation 6 relates the amplifier input voltage to the position output of the moving coil. The amplifier gain, k_a, is obtained from the specification [10]; the thrust constant, k_m, is determined by measuring the electromagnetic force versus the constant current; the viscous damping coefficient, c, is determined by measuring the rate of decay of oscillation; and the complex spring constant k is determined by measuring the complex spring force versus displacement. The values for the model parameters are shown in Table 1.

The comparison of the measured and simulated response at 1-V-step command signals applied to the input of the amplifier is shown in Fig. 7. It can be seen that the simulated response of the second-order model matches the measured response well.

Table 1 Model parameters

Parameter name	Value
Amplifier gain, k_a	1.6 A/V
Thrust constant, k_m	12.325 N/A
Mass of moving parts, m	0.32 kg
Damping coefficient, c	14.51 N.s.m^{-1}
Complex spring constant, k	4,980 N/m

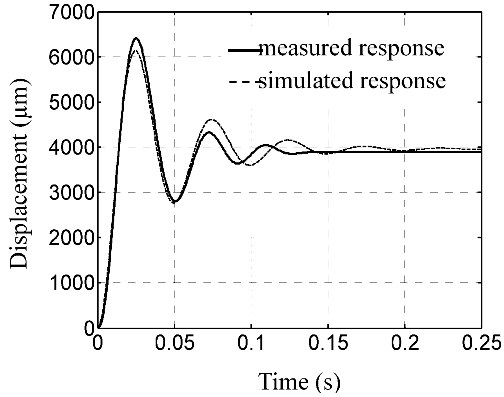

Fig. 7 Comparison of the measured and simulated responses at 1-V-step command signals

4 Design of controllers

To achieve good tracking performance, a PID feedback controller with incomplete derivative and a feedforward controller are employed in the control system, as shown in Fig. 8. The feedback controller guards stability and improves disturbance rejection, while the feedforward controller improves tracking performance. In Fig. 8, x_c, e, u_i, and x denote the command position, servo error, plant input, and plant output, respectively.

4.1 Feedback controller

The transfer function of the PID controller including a low-pass filter with the derivative term is expressed as:

$$\begin{aligned} U_{fbk}(s) &= \left(K_P + \frac{K_P}{T_I s} + \frac{K_P T_D s}{1+T_f s}\right)E(s) + u_0 \\ &= U_P(s) + U_I(s) + U_D(s) + u_0 \end{aligned} \tag{7}$$

where $U_{\text{fbk}}(s)$ is the feedback controller output, K_P is the proportional gain, T_I is the integral time constant, T_D is the derivative time constant, $T_f = T_D/N$ is the time constant, and N=10 is the filter factor for the derivative term [11], $E(s)$ is the position error between the command and output, and u_0 is the initial control value. The discrete-time PID controller with finite-gain derivative is given in Eq. 8:

$$\begin{aligned} U_{fbk}(k) &= u_P(k) + u_I(k) + u_D(k) + u_0 \\ &= K_P e_k + K_I \sum_{j=0}^{k} e_j + u_D(k) + u_0 \end{aligned} \tag{8}$$

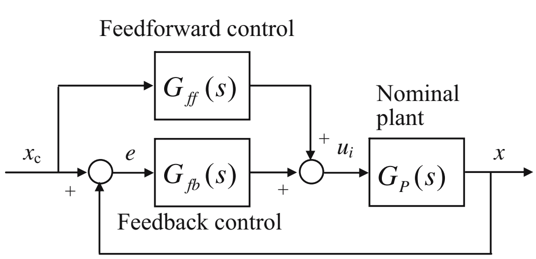

Fig. 8 Block diagram of the control system

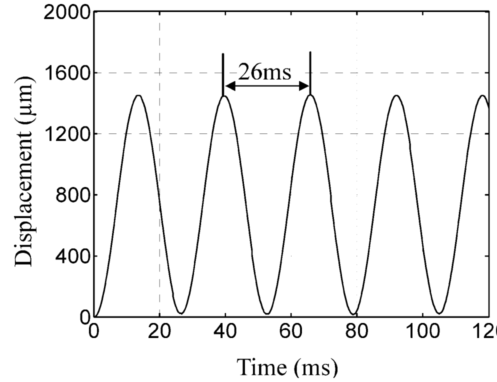

Fig. 9 Measured continuous oscillation curve

Table 2 Initial PID parameters

K_P	T_I	T_D	K_I	K_D
$0.6K_{\text{cr}}$	$0.5P_{\text{cr}}$	$0.125P_{\text{cr}}$	$K_P\ (T/T_I)$	$K_P\ (T_D/T)$
2.53	13	3.25	0.039	41.11

Table 3 Final PID parameters

K_P	K_I	K_D
8.83	0.191	201.19

where $K_I = K_P T/T_I$ is the integral gain and T is the sampling period. The $u_D(k)$ term is given as follows:

$$u_D(k) = K_D(1-\alpha)(e_k - e_{k-1}) + \alpha u_D(k-1) \tag{9}$$

where $K_D = K_P T_D/T$ is the derivative gain and $\alpha = T_f/(T_f + T)$.

An effective initial design of achieving the parameters of the PID controller was performed on a real plant by the Ziegler-Nichols oscillation method. Figure 9 shows the measured continuous oscillation curve. In Fig. 9, the proportional controller critical gain K_{cr}=4.22, the critical oscillation period of the plant output P_{cr}=26 ms, and the

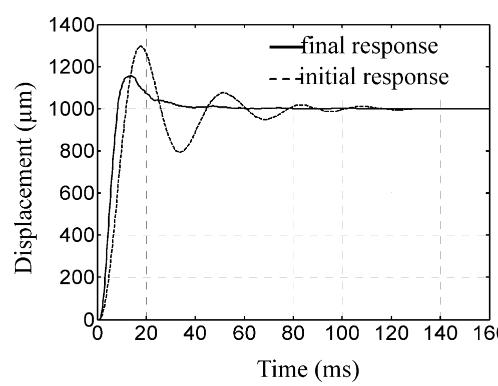

Fig. 10 Measured closed-loop step response for 1,000-μm command position

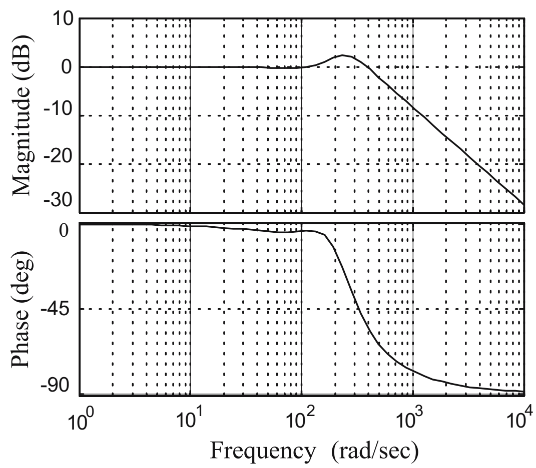

Fig. 11 Closed-loop frequency response with the PID controller

sampling time T=0.2 ms. The initial PID parameters based on the rules of the Ziegler-Nichols control algorithm are given in Table 2. Then, the PID parameters can be adjusted to obtain a good closed-loop response for the control system. If the overshoot is less than 16%, the rise time is less than 8 ms, and the settling time is less than 30 ms, the final PID parameters can be determined as shown in Table 3. The measured closed-loop step response curves with the initial and final PID parameters are shown in Fig. 10. Figure 11 shows the closed-loop frequency response with the PID controller, whose bandwidth is approximately 80 Hz.

4.2 Feedforward controller

In order to minimize the tracking error, a common strategy is to make the product of the plant and the feedforward controller unity, hence, to find a feedforward controller that equals the plant's inverse. The feedforward controller can be expressed as:

$$G_{ff}(s) = \frac{1}{G_P(s)} = \frac{ms^2 + cs + k}{k_a k_m} \tag{10}$$

Table 4 Motor specifications

Items	Values
Overall dimensions	175×92×92 mm^3
Magnetic flux density, B_δ	0.591 T
Coil inductance, L	1.298 mH
Coil resistance, R	2.21 Ω
Number of coil windings, N	238
Coil average length of each turn, l	201 mm
Axial length of magnets	18 mm
Axial length of moving coil	40 mm
Mass of mover (no load)	0.26 kg

Table 5 Servo amplifier specifications

Input power voltage	16 to 48 V DC
Signal input voltage range	±10 V DC
Continuous output current	8 A
Peak output current	16 A
Gain current mode	1.6 A/V
Current monitor output	4 A/V

This controller must ultimately be implemented in discrete time. A first-order backwards difference approximation is given by the following substitution [12]:

$$s = \frac{z-1}{zT} = \frac{1-z^{-1}}{T} \tag{11}$$

So, it results in the following discrete-time transfer function for the feedforward controller:

$$G_{ff}(s) = \frac{m}{k_a k_m}\left(\frac{1-2z^{-1}+z^{-2}}{T^2}\right) + \frac{c}{k_a k_m}\left(\frac{1-z^{-1}}{T}\right) + \frac{k}{k_a k_m} \tag{12}$$

Fig. 12 Configuration of the linear drive system

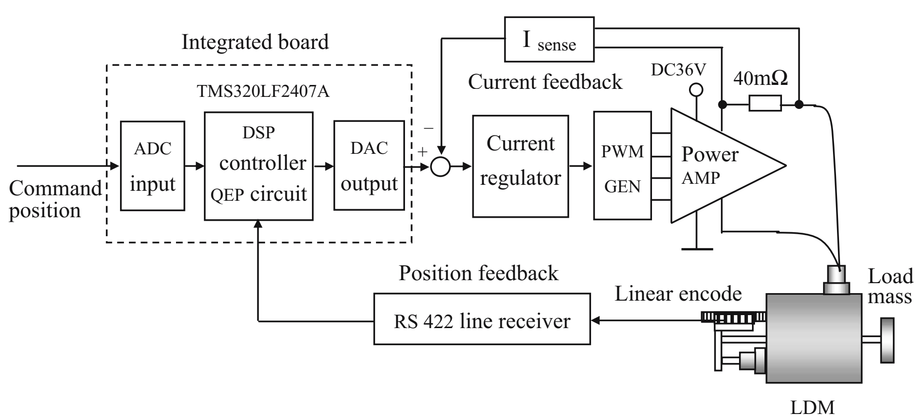

Table 6 Linear encoder specifications

Scanning head dimensions	34×13.2×12.4 mm^3
Accuracy	±5 μm
Resolution	1 μm
Max. allowable velocity	480 m/min

5 Tracking performance test

5.1 Experimental setup

The configuration of the linear drive system is shown in Fig. 12. It consists of a moving-coil type LDM, a commercial pulse-width modulated servo amplifier, KXA-48-8-16, made by Kollmorgen, a linear optical encoder, LIE52PL5GD0, made by Numerik Jena, and a TMS320LF2407A digital signal processor (DSP) board which includes an A/D converter, a D/A converter, and a quadrature encoder pulse (QEP) circuit. The specification for the motor, the servo amplifier, and the linear encoder are shown in Tables 4, 5, and 6, respectively. Figure 13 is a photograph of the experimental setup.

5.2 Tracking performance

The input motion command chosen for tracking performance evaluation is the triangular wave (frequency 4 Hz, amplitude 5,000 μm). The output position is measured from the linear optical encoder installed in the LDM with a 0.2-ms sampling period. The measured position error with or without the feedforward controller is shown in Figs. 14 and 15, where the solid and dashed lines indicate the input signals and output response, respectively. It is clear that, with the feedforward controller, the system output response has a small tracking error (within ±14 μm), while without the feedforward controller, the position errors are approximately ±110 μm. The two experiments have proved the effectiveness of the feedforward control algorithm proposed in this paper.

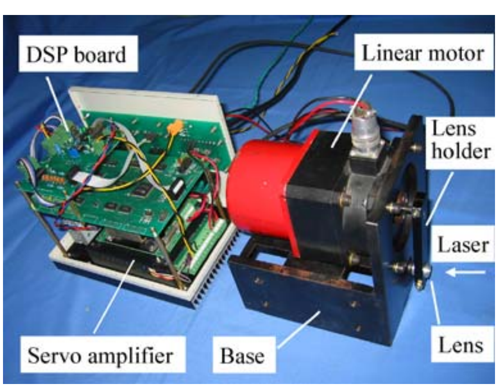

Fig. 13 Experimental setup

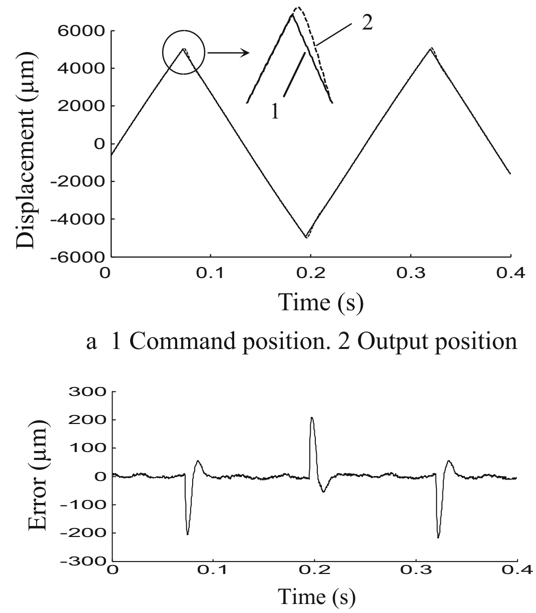

a 1 Command position. 2 Output position

b Tracking error

Fig. 14 a, b Measured position and position error with the feedforward controller. **a** Command position (*1*) and output position (*2*). **b** Tracking error

6 Conclusions

This paper presents a linear drive system of the dynamic focus module using the moving-coil PM linear DC motor. A digital signal processor (DSP) based digital–analog mixed dual closed-loop (position loop and current loop) position control system is constructed. The dynamic model of the linear DC motor (LDM) and the transfer function of

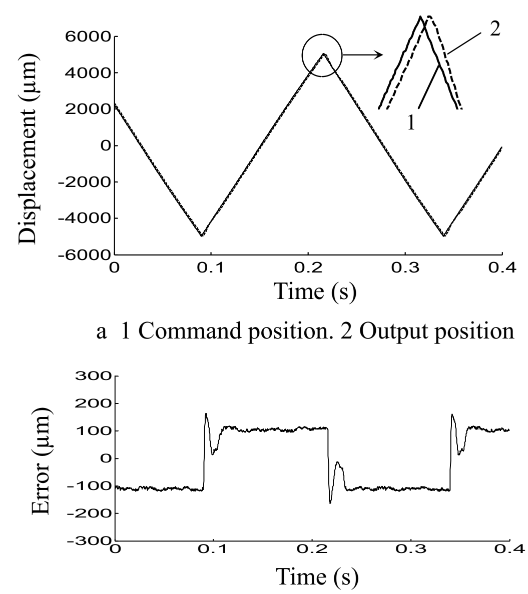

a 1 Command position. 2 Output position

b Position error

Fig. 15 a, b Measured position and position error without the feedforward controller. **a** Command position (*1*) and output position (*2*). **b** Tracking error the control system are derived, and the PID feedback controller including a low-pass filter with the derivative term plus a feedforward digital controller is designed. The contrastive experiments have verified the effectiveness of the proposed control algorithm. The linear drive system has fast dynamic response and acceptable tracking error. The linear drive system tested in this research can replace the rotary-to-linear conversion mechanism for the driving dynamic focus module of selective laser sintering (SLS) machines.

Acknowledgements This project is supported by the National Natural Science Foundation of China (grant no. 60474021) and National 863 Hi-Tech. Program of China (grant no. 2002AA423120). The authors would like to express their special thanks to Prof. Liu Yi from the English Department, Huazhong University of Science and Technology, China, for his patient help in the proofreading of the paper.

References

1. Xie J, Huang SH, Duan ZC, Shi YS, Wen SF (2005) Correction of the image distortion for laser galvanometric scanning system. J Optics Laser Technol 37(4):305–311
2. Xie J, Duan ZC, Shi YS (2004) Study on key technologies for galvanometer scanning system used in selective laser sintering (in Chinese). J Manuf Autom 26(4):9–13
3. GSI Lumonics (1996) Post-objective scanning variable field systems. HPLK Series User's Manual
4. Madni, AM, Vuong JB, Lopez M, Wells RF (2002) A smart linear actuator for fuel management system. In: Proceedings of 5th Biannual IEEE World Automation Congress (WAC 2002), Orlando, Florida, June 2002, vol 14, pp 615–624
5. Lequesne B (1996) Permanent magnet linear motors for short strokes. IEEE Trans Ind Appl 32:162–170
6. Mikhaeil-Boules N (1995) Design and analysis of linear actuator for active vibration cancellation. In: Proceedings of the 30th IEEE-IAS Annual Meeting (IAS'95), Orlando, Florida, October 1995, vol 1, pp 469–475
7. Bang Y-B, Lee K-M (2004) Linear motor for ejector mechanism. Int J Adv Manuf Technol 24(7–8):582–589
8. Yajima H, Wakiwaka H, Minegishi K, Fujiwara N, Tamura K (2000) Design of linear DC motor for high-speed positioning. Sens Actuators A Phys 81(1–3):281–284
9. Electro-craft Corporation (1977) DC motors, speed controls, servo systems: an engineering handbook. Pergamon Press, New York
10. PWM Servo Amplifiers (2003) KXA Series User's Manual
11. Ang KH, Chong G, Li Y (2005) PID control system analysis, design, and technology. IEEE Trans Contr Syst Technol 13 (4):559–576
12. Wei ZH, Schinstock DE (2005) Feedforward control strategies for tracking performance in machine axes. Chinese J Mech Eng 18(1):5–9